International Communications in Heat and Mass Transfer 138 (2022) 106353

Contents lists available at ScienceDirect

International Communications in Heat and Mass Transfer

journal homepage: www.elsevier.com/locate/ichmt

Chemical reaction influence on nanofluid flow in a porous layer: Stability analysis

J.C. Umavathi [a], M.A. Sheremet [b,*]

[a] Department of Mathematics, Gulbarga University, Gulbarga 585 106, Karnataka, India
[b] Laboratory of Convective Heat and Mass Transfer, Tomsk State University, Tomsk 634050, Russia

ARTICLE INFO

Keywords:
Thermo-solutal convection
Stability
Nanofluid
Exothermic reaction
Frank–Kamenetskii thermal ignition
Porous medium
Brownian motion
Thermophoresis

ABSTRACT

An influence of exothermic chemical reaction on the natural thermo-solutal convection in a horizontal channel filled with sparsely packed permeable nanofluid is investigated. It is assumed that the fluid viscosity is different from the effective viscosity. The Brinkman approach is engaged for the porous material, while the nanofluid approach features the Buongiorno model. To figure out the stability of the linear terms, normal mode analysis is opted. Galerkin technique is selected to work out the nonlinear terms. The Rayleigh number and its relevant wave numbers are assessed for all dimensionless parameters and exposed in the form of graphs. It is found that there is a critical value of Frank–Kamenetskii number at which the system is most unstable. It is found that increasing the viscosity ratio delays the onset of convection. With exothermic chemical reactions, the fluid in the porous medium is more prone to instability as compared to the case in which chemical reactions are absent. A critical value of Frank–Kamenetskii number is also identified at which the system is most unstable, and this is shown to be independent of both porous media parameter and the viscosity ratio. Applications of the study arise in nano-doped geothermal energy extraction, chemical and bio reactors and other engineering systems.

1. Introduction

Conventional methods employed to increase heat transfer rates in industrial and energy systems, which include extended surface areas and micro-channels, are characterized by the disadvantage that when the required pumping power of the cooling liquid is increased or when micro fluids are deployed, gravity settling, clogging and other sedimentation problems arise. The innovative concept of 'nanofluids' consisting of base fluid having nanoparticles suspensions is the best choice to overcome these challenges. By dispersing metallic (e.g. silver oxide, copper, zinc) or non-metallic (carbon nanotube, silicate etc) nano-sized particles or nano fibres having a typical size of <100 nm in a fluid results in nanofluid. These nanofluids can be employed in the extraction of the geothermal energy [1]. Further when drilling, nanofluids reduce the temperature and friction which occurs in machinery equipment working. By placing nanoparticles in geothermal fields, demonstrating that as circuit fluids, copper or alumina nanofluids yield enhanced heat extraction rates compared with conventional steam or water systems [2,3]. Nanofluids simultaneously avoid the flooding and agglomeration problems encountered with conventional displacement fluids. In such systems porous media are encountered and natural rock (stratum) boundaries arise. The exceptional thermal conductivity enhancement achieved with nanofluids makes them a viable technology for geothermal power systems.

The approach is defined to replicate the onset of convection due to exothermic reactions saturated by a nanofluid, as a simulation of a reactive geothermal system. Thermosolutal convection and reactive flows are significant in geothermal systems [4–9]. In certain reactive flows, density differences in a liquid mobilize thermal convection which occurs to release the heat of an exothermic reaction and this in turn disturbs the reaction rate. Such a complicated interaction between convection and reaction is the major aspect for different instabilities monitored in reacting flows. In few cases including the storing of self igniting media such as waste dumps, coal piles, etc., these non-uniform motions are considered to be responsible for preventing heat explosions, while in other cases, these non-uniform flows, as in a reaction in a packed bed, can lead to an appearance of hot spots and should be avoided. Exothermic reactions can be influenced in a critical way by the properties of the natural convection. Chemical vapor deposition systems, synthesis of ceramic media by self-propagating reactions, tubular laboratory reactors, geochemical processes in reservoirs, oxidation of solid media in large chambers are among some of the representative examples of the influence of chemical reactions on natural convection

* Corresponding author.
E-mail address: Michael-sher@yandex.ru (M.A. Sheremet).

https://doi.org/10.1016/j.icheatmasstransfer.2022.106353

Available online 9 September 2022

Nomenclature

a	dimensionless wave number
b, d	reaction orders
B	pre-exponential factor
D_B	Brownian motion parameter
D_T	thermophoresis parameter
E	activation energy (J)
FK	Frank–Kamenetskii parameter
g	gravitational acceleration vector (m/s^2)
H	height of the porous layer (m)
K	permeability (m^2)
Kr	viscosity ratio
l, m	dimensionless wave number in the x- and y- coordinates
Ln	thermo-nanofluid Lewis number
M	thermal capacity ratio
N_A	modified diffusivity ratio
N_B	modified particle-density rise
p	pressure (Pa)
Pr	Prandtl number
q	velocity vector (m/s)
Q	heat of reaction (kJ/mol)
R	the universal gas constant (J/K.mol)
Ra	modified Rayleigh number
Rm	basic-density Rayleigh number
Rn	nanoparticle concentration Rayleigh number
T	temperature (K)
t	time (s)
(u,v,w)	velocity components (m/s)
(x,y,z)	space coordinates (m)
Y_F^b, Y_0^d	mass fraction of fuel and oxidizer respectively

Greek symbols

κ	effective heat diffusivity (m^2/s)
β	heat expansion parameter (K^{-1})
ε	porosity
μ	dynamic viscosity (kg/m.s)
μ_e	effective viscosity (kg/m.s)
ν	kinematic viscosity (m^2/s)
ν_e	effective kinematic viscosity (m^2/s)
θ	non-dimensional temperature
ρ	density (kg/m^3)
σ	porous parameter

Superscripts

*	non-dimensional quantity
′	perturbed quantity

Subscripts

b	base state quantity
r	reference

flows. Articles are published using the Frank–Kamenetskii thermal explosion model [9] which was in use for a homogeneous mixture of reactants within an enclosure with isothermal boundaries. Law and Law [10] used matched asymptotic expansions to calculate the weakly reactive ignition in steady boundary-layer motion of a combustible mixture over heated, isothermal, non-permeable, non-catalytic flat sheet at large activation energy. Li et al. [11] derived a locally similar solution for thermal ignition of a reacting boundary-layer motion about the hot wedge/cone surface. Bég et al. [12] engaged DTM and Padé approximants to simulate the thermal ignition in combusting flow from a tilted slope as a model of forest fire spread, evaluating achievement of Frank–Kamenetskii parameter on thermal buoyancy effects. Further studies employing the Frank–Kamenetskii theory include Bég et al. [13] (on elastico-viscous hypergolic bi-propellant rocket fuel conduction-convection at different Biot numbers). Hashmi et al. [14] presented homotopy results for thermal source/sink influences in mixed convective hydromagnetic Oldroyd-B fluid in the gap between two infinite stretching disks of constant temperature. They computed the thermal and momentum components using Frank–Kamenetskii parameter. Gordon [15] researched on the analytical approach of heat explosion in Darcy porous media. Several researchers have also considered free convection in nanofluid immersed porous matrix for the thermal ignition. Rahman et al. [16] estimated the natural magneto-convection flow energized with Frank-Kamenstkii reaction and Arrhenius kinetics for the permeable nanofluid. They noted that both Rayleigh and Frank-Kamenetskii numbers exert a significant impact on the convective patterns and that average Nusselt number is elevated with Frank-Kamenetskii parameter (stronger exothermic reaction) whereas it is suppressed with Rayleigh number. Ul-Haq [17] investigated the exothermically reactive convection for the conducting permeable nanofluid in the triangular cavity, observing that exothermic reaction produces more heat with higher Frank-Kamenetskii parameter, and significantly intensifies the circulation with the enclosure. Relatively sparse studies have been organized for the presence of exothermic reaction with considerations of nanoparticles and thermo-solutal instability. The interaction of chemical reaction and buoyancy forces was first considered by Kordylewski and Krajewski [18] for the permeable fluid. They assumed LTE (local thermal equilibrium) model and a zero-order exothermic reaction with a Darcy law under the Boussinesq approximation. They bestowed the consequence of chemical reaction on the critical conditions of heat ignition. Gatica et al. [19] presented stability test of chemical reaction outcome on thermal convection in a confined permeable fluid. They considered first order isothermal and zeroth order and non-isothermal reaction and analytically evaluated the Rayleigh number. Vafai et al. [20] reported finite element simulations of time-dependent convection along with chemical reactions in a packed bed. They resolved the critical boundary temperature producing thermal runaway inside the cavity applying Frank-Kamenetskii theory. They also identified “hot spots” in domains removed from the horizontal borders of the chamber. Subramanian and Balakotaiah [21] explored the conditions to set on the exothermic reactions in an open rectangular cavity embedded with porous matrix. They demonstrated the sensitivity of bifurcation neutral stability lines on Lewis number, observing a displacement in steady stability border with higher Ra. They further identified a critical Lewis number below which the entire ignited conduction branch is stable to convective perturbations Rayleigh number at the extinction point. Malashetty et al. [22] have inspected the impact of exothermic reactions on the onset of convection for the permeable liquid adopting Darcy's law.

The papers mentioned as above adapted the Darcy law for the momentum equation. However, Darcy's model is applicable only under special circumstances and is confined to viscous-dominated, low speed flows for which a bulk matrix impedance alone is present. More generalized models for evaluating accurately convection flows in porous beds are however available which may address inertial, channeling, tortuosity, vorticity diffusion and other effects. An elegant formulation is the Darcy-Brinkman model which includes the Brinkman's viscous term and has been described in some detail by Kladias and Prasad [23]. Vasseur and Robillard [24] discussed the stability for the porous matrix enclosure convection with variable temperature gradients adopting the Darcy-Brinkman model which was shown to achieve a better prediction for the diffusion. Bég et al. [25] utilized a non-Darcy model to

understand the viscous effects in two-dimensional laminar boundary layer flows in homogenous porous media. Kumar et al. [26] applied the Darcy-Brinkman model and both perturbation and differential transform methods to calculate the influence of mixed convection characteristic, porous characteristic, relative viscosity parameter, aspect parameter, relative conductivity parameter and Biot numbers in a duct with mixed boundary conditions. Tripathi and Bég [27] deployed a homotopy perturbation method (HPM) to investigate the peristaltic propulsion of Maxwell viscoelastic biopolymers in incompressible Darcy-Brinkman porous media.

The magnetic impacts on the mixed convection of a nanofluid in an undulating porous cavity under the thermal radiation and heat generation effects were researched by Alsedais et al. [28] under LTNE (linear thermal nonequilibrium) approach. Their results indicated that the growth in nanoparticles parameter augments the profiles of average Nusselt number of a fluid phase. The heat transfer was influenced by the variations in the length/position of the heater source. Aly and El-Sapa [29] studied more complex problem by introducing magnetohydrodynamic thermosolutal convection of a nanofluid in a square cavity including dual rotation among an outer circular cylinder and an inner cross shape. They remarked that the variations of the thermal/solutal boundary conditions can work effectively in adjusting the heat/mass transfer and nanofluid flow within a cavity. Further increasing Hartmann number from 0 to 50 lessens the maximum of the nanofluid velocity by 44.4%. Aly et al. [30] adopted the time-fractional derivative of the incompressible smoothed particle hydrodynamics (ISPH) method for studying the magnetic field, diffusion-thermo, and thermo-diffusion impacts on the double diffusion of a nanofluid in a porous annulus between a square cavity and astroid element. The main findings of the ISPH numerical simulations showed that a decrease in a fractional derivative order delivers the sooner steady-state of the double diffusion which suppresses the performed calculations. Alsedais and Aly [31] also worked on the double-diffusive convection from an oscillating baffle embedded in an astroid-shaped cavity suspended by nano-encapsulated phase change materials using ISPH simulations. They found that the Stefan and fusion parameters were acting effectively in enhancing a phase change zone. The superior values of the average Nusselt and Sherwood numbers were obtained when the inner baffle was expanded due to higher buoyancy forces.

The instability properties of mixed convection flow of different nanofluids in a differentially heated vertical channel through a linear stability analysis were reported by Singh and Khandelwal [32]. Their main findings were that compared to conventional pure water fluid, the inclusion of nanoparticles in pure water delayed the onset of instabilities by reducing the growth of the disturbance. The oscillation characterstics and evolution process for large Prandtl number ($Pr = 58$) nanofluid thermocapillary convection and the variation of critical Marangoni number and flow instability under different nanoparticle concentrations were reported by Zhou et al. [33]. Their results showed that, nanofluid thermocapillary oscillatory convection is consisted of multiple vortices and these vortices migrate periodically from cold wall to hot wall. Further as nanoparticle volume fraction increases, the critical Marangoni number decreases. In order to reveal the oscillatory characteristics of the natural convection of nanofluid, Hu et al. [34] presented a comprehensive numerical work on the oscillatory natural convection of Al_2O_3-water nanofluid near its density maximum in a narrow horizontal annulus. Their results showed that the density inversion of the working fluid affected the velocity and temperature distributions of the natural convection of Al_2O_3-water nanofluid significantly. Adding nanoparticles was beneficial to stabilizing the flow of nanofluid and keeping the symmetry of the flow structure. Weak nonlinear hydrodynamic thermal instability analysis has been performed by Bhadauria and Kiran [35] for double diffusive oscillatory mode of convection in a horizontal layer of viscoelastic fluid, heated from below. They found that in-phase temperature modulation has negligible effect, while out of phase temperature modulation and only lower plate temperature modulation have oscillatory effects on heat and mass transport.

The Darcy-Brinkman model is picked in the conservation balance equation to understand the instability in permeable nanofluid. The liquid viscosity and the effective viscosity are different for the fluid in porous media. The formation of multiple conductive states and the heat rate result to the marked differences between the reaction-driven convection and the classical Lapwood-Brinkman and Rayleigh-Bénard convection. More recently, the focus is on trying to study the convective instabilities that arise due to exothermic reactions occurring inside a porous medium. The heat released by an exothermic reaction creates density differences within the fluid and induces natural convection, which in tern, affects the rate of reaction. This complex interaction between convection and chemical reaction is believed to be a major factor in different instabilities observed in reacting flows. These non-uniform flows, in some cases, as in a chemical reaction in a packed bed, might lead to the formation of hot spots and are to be avoided, while in some other cases, like the storing of self igniting materials such as coal piles, waste dumps, etc., these non-uniform flows are believed to be responsible for preventing (or delaying) thermal explosions. Natural convection effects may influence the course of an exothermic chemical reaction in a critical way. Examples of the interaction of chemical reaction and free convection occur in tubular laboratory reactors, chemical vapor deposition systems, oxidation of solid materials in large containers, synthesis of ceramic materials by self-propagating reaction, and others. However few works have been done on the effect of chemical reaction on convection in porous media until recently. The present review is particularly relevant to chemo-dynamic simulations of nano-doped geothermal reservoirs and also in simulating operations of an exothermic reactor during its shutdown period. It may also be of relevance to porous media combustion fuel cell systems [36,37]. The major contribution of the proposed analysis is to examine the enforcement of the Frank–Kamenstkii thermal ignition parameter and nanoscale influences on onset of convection in using a Darcy-Brinkman model filled with reacting nanofluid in a horizontal duct. Extensive linear stability computations with Fourier decomposition are presented and a parametric study of the impingement of key parameters on transport characteristics conducted with graphical visualizations.

2. Exothermic reactive nanofluid porous media model

The schematic figure consists of horizontal duct filled with nanofluid along with the porous bed as exhibited in Fig. 1. The lower wall is located at $z = 0$ and the upper plate at $z = H$ with the z-axis in the vertical direction against gravity. It is estimated that the inert porous nanofluid is chemically reactive and the exothermic reactions are weak (Frank-Kamenetskii thermal ignition model) and is cooled from the top boundary (representing e.g. the rock stratum of a geothermal reservoir or upper wall of a reactor) at a temperature of T_c. The Newton's balance equations are as follows [41].

$$\nabla q = 0 \tag{1}$$

$$\rho_0\left(\varepsilon^{-1}\frac{\partial q}{\partial t}+\varepsilon^{-2}q\nabla q\right) = -\nabla p+\rho g-\frac{\mu}{k}q+\mu_e\nabla^2 q \tag{2}$$

$$\begin{aligned} M\frac{\partial T}{\partial t}+q\nabla T \;&= k\nabla^2 T+QBY_F{}^{b}Y_0{}^{d}exp\left(-\frac{E}{RT}\right)\\ &\quad+\frac{\varepsilon(\rho c)_p}{(\rho c)_f}\left[D_B\nabla\phi\nabla T+D_T\frac{\nabla T\nabla T}{T_0}\right] \end{aligned} \tag{3}$$

$$\frac{\partial \phi}{\partial t}+\varepsilon^{-1}q\nabla\phi = \nabla\left[D_B\nabla\phi+D_T\frac{\nabla T}{T}\right] \tag{4}$$

$$\rho = \phi\rho_p+(1-\phi)\rho_0[1-\beta(T-T_C)] \tag{5}$$

Zero order reactions are possible in two ways. The first possibility is the case of $b = d = 0$, which inform that the concentrations of reactants

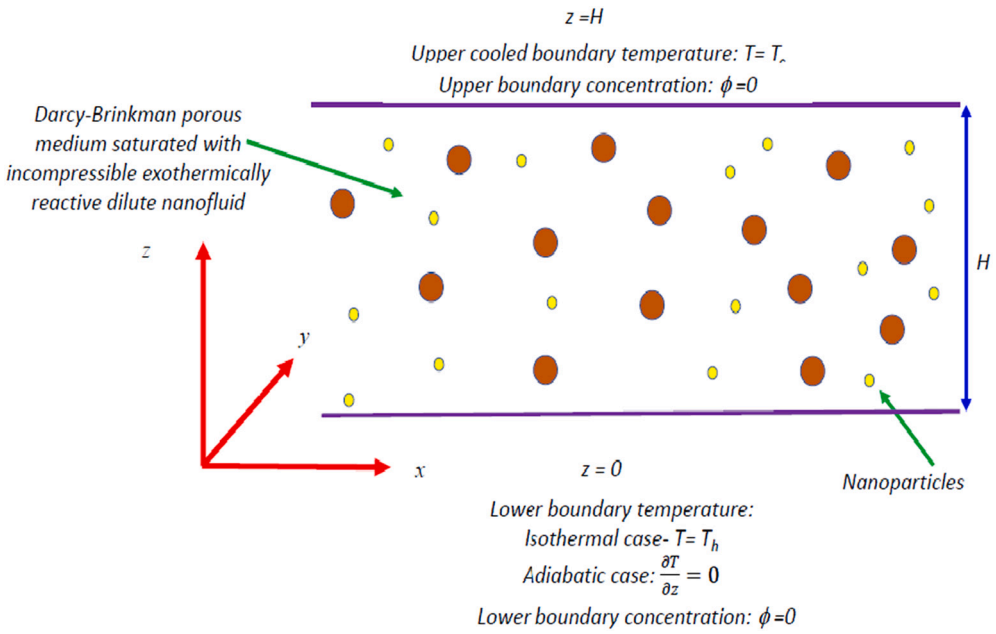

Fig. 1. Reactive nanofluid porous medium model.

do not play any role in the chemical reaction. This is not physical due to it signifies that chemical reaction is possible without the reactants. Nest case is that only a low reactant concentration is depleted during the reaction, which characterizes the weakly reacting situation under low temperature variation and is therefore the case addressed in the present work. The Boussinesq approximation is supported because the discrepancy in the temperature is not large. The Boussinesq approximation was widely utilized in many studies e.g. Stroh and Balakotaiah [38], Subramanian and Balakotaiah [39]. To summarize, the current mathematical model is established on the following assumptions:

1. The nanofluid is chemically reactive fluid and process weakly exothermic chemical reaction of order zero.
2. During the reaction a low reactant concentration is depleted illustrating the weakly reacted situation in a circulation with low temperature differences.
3. The fluid is subjected to large activation energy reaction.
4. Boussinesq approximation is invoked; the liquid and the solid matrix are in heat equilibrium.
5. The fluid viscosity and effective Brinkman viscosity are not equal.

The heat border condition at the upper wall is

$$T(x,y,H) = T_C \tag{6}$$

For the lower temperature border condition, we assume two various cases, a wall with constant temperature and a thermally-insulated wall. The conditions on the walls for the temperature for these two cases are:

Case (i) a wall of constant temperature:

The lower boundary wall using isothermal condition is

$$T(x,y,0) = T_h \text{ where } T_h > T_C \tag{7}$$

Case (ii) a thermally-insulated wall:

For an adiabatic wall at the bottom the boundary condition is

$$\frac{\partial T(x,y,0)}{\partial z} = 0 \tag{8}$$

High activation energy reaction is enforced and hence we have $RT_C/E << 1$. With this condition and setting $M = 1$, eq. (3) can be simplified to

$$\frac{\partial \theta}{\partial t} + q\nabla T = k\nabla^2\theta + Cexp(\theta) + \frac{\Phi(\rho c)_p D_B \phi_r}{(\rho c)_f}\nabla\phi\nabla T + \frac{\Phi(\rho c)_p D_T \phi_r T_r}{(\rho c)_f T_C}\nabla T\nabla T \tag{9}$$

where $C = QBY_F{}^b Y_0{}^d exp(-E/RT_C)$, $\theta = (T - T_C)/T_r$, $\Phi = (\phi - \phi_C)/\phi_r$ with $Tr = RT_C^2/E$ being the reference temperature. Zero concentration is imposed at both boundaries. The dimensionless concentration and temperature are Φ and θ.

The conditions on the walls in terms of θ, reduce to:

$$\theta(x,y,H) = 0 \tag{10}$$

$$\theta(x,y,0) = \theta_h \text{ or } \frac{\partial \theta}{\partial z}(x,y,0) = 0 \tag{11}$$

where $\theta_h = (T_h - T_C)E/(RT_C{}^2)$.

2.1. Basic state

The basic undisturbed state corresponding to two various lower wall border conditions are taken into account on the temperature. In the undisturbed state, one can find

$$q_b(u,v,w) = (0,0,0), \theta = \theta_b(z), p = p_b(z), \rho = \rho_b(z) \tag{12}$$

Eqs. (2) and (9) become:

$$\nabla p_b(z) + \rho_b(z)g = 0 \tag{13}$$

$$\frac{d^2\theta_b}{dz^2} + \left(\frac{C}{\kappa}\right)\left(\frac{E}{RT_C{}^2}\right)exp(\theta_b) = 0 \tag{14}$$

where $\theta_b = (T_b - T_C)E/(RT_C^2)$. The concentration eq. (4) becomes

$$\frac{d^2\Phi_b}{dz^2} + \frac{D_T T_r}{D_B T_C \phi_r}\frac{d^2 T_b}{dz^2} = 0 \tag{15}$$

The dimensionless form of Eq. (14) is

$$\frac{d^2\theta_b}{dz^{*2}} = -FKexp(\theta_b) \tag{16}$$

Here $z^* = z/H$ is dimensionless vertical coordinate and $FK =$

$C\left(\frac{H^2}{\kappa}\right)\left(\frac{E}{RT_C^2}\right)$ is the Frank-Kamenetskii number (also known as the reduced Damkohler number in the combustion literature). The Frank-Kamenetskii parameter is the ratio of characteristic circulation time to the characteristic reaction time. (For simplicity asterisks will not be mentioned in future). The exact solution of Eq. (16) is given by:

$$\theta_b = ln\left(\frac{C_1}{2FK}\right) + ln\left[1 - \left(\frac{1 - C_2 e^{-\sqrt{C2}\, z}}{1 + C_2 e^{-\sqrt{C2}\, z}}\right)^2\right] \tag{17}$$

for $FK \neq 0$, where C_1 and C_2 are the integration parameters to be defined.

For Case (i), using the boundary conditions of constant temperature

$$\theta_b = \theta_h \text{ at } z = 0 \text{ and } \theta_b = 0 \text{ at } z = 1 \tag{18}$$

C_1 and C_2 are emerg0ed implicitly as

$$e^{\sqrt{C_1}}\left[\frac{1 - (1 - 2FK/C_1)^{0.5}}{1 + (1 - 2FK/C_1)^{0.5}}\right] = \left[\frac{1 - (1 - 2FKexp(\theta_h)/C_1)^{0.5}}{1 + (1 - 2FKexp(\theta_h)/C_1)^{0.5}}\right] \tag{19}$$

and

$$C_2 = e^{\sqrt{C_1}}\left[\frac{1 - (1 - 2FK/C_1)^{0.5}}{1 + (1 - 2FK/C_1)^{0.5}}\right] \tag{20}$$

In eq. (20), C_1 is a function of FK and θ_h.

For Case (ii), the border conditions employed are

$$\frac{d\theta_b}{dz} = 0 \text{ at } z = 0, \quad \theta_b = 0 \text{ at } z = 1 \tag{21}$$

We then determine C_1 and C_2 which yield

$$e^{\sqrt{C_1}}\left(1 - \sqrt{1 - 2FK/C_1}\right) = \left(1 + \sqrt{1 - 2FK/C_1}\right) \text{ and } C_2 = 1 \tag{22}$$

Detailed evaluation of ignition conditions is omitted as the critical conditions of thermal ignition was reported by many other authors (see e.g. Malashetty and Gaikwad [40]). Accordingly, we focus attention on investigating only the stability of the base state solutions.

3. Linear stability analysis

Perturbing basic state quantities such as velocity, pressure, density and temperature yields:

$$q = (u', v', w'), p = p_b + p', \rho = \rho_b + \rho', \theta = \theta_b + \theta' \tag{23}$$

Here the primes define weak perturbations from the undisturbed state. Substituting Eq. (23) into Eqs. (1)–(3), the pressure is eliminated, using the equation of state and neglecting nonlinear terms become

$$\frac{\partial}{\partial t}\varepsilon^{-1}\nabla^2 w' = -\frac{\nu}{\kappa}\nabla^2 w' + \nu_e \nabla^4 w' + g\beta Tr \nabla_1{}^2\theta' - g\left(\frac{\rho_p}{\rho_0} - 1\right)\nabla_1{}^2\Phi' \tag{24}$$

$$\frac{\partial \theta'}{\partial t} + w'\frac{\partial \theta_b}{\partial z} = \kappa\nabla^2\theta' + Cexp(\theta_b)\theta' \tag{25}$$

$$\varepsilon^{-1}\frac{\partial \Phi'}{\partial t} + w' = D_B\nabla^2\Phi' + \frac{\Phi'(\rho c)_p D_T \phi_r T_r}{(\rho c)_f T_C}\nabla^2 T' \tag{26}$$

Here $\nabla_1{}^2 = \left(\frac{\partial^2}{\partial x^2} + \frac{\partial^2}{\partial y^2}\right)$, $C = QBY_F{}^a Y_0{}^b exp(-E/RT_C)$.

Eqs. (24)–(26) can be expressed in non-dimensional form using the following quantities:

$$w^* = \frac{w'H}{\kappa}, (x^*, y^*, z^*) = \frac{(x,y,z)}{H}, t^* = \frac{\kappa t}{H^2}, Kr = \frac{\mu_e}{\mu}, Pr = \frac{\nu\varphi}{\kappa}, \sigma^2 = \frac{H^2}{\kappa},$$
$$Ra = \frac{(1-\phi_c)\beta g H^3 T_r}{\nu\kappa}, Rn = \left(\frac{\rho_p}{\rho_0} - 1\right)\frac{\beta g H^3 T_r}{\nu\kappa}, FK = C\left(\frac{H^2}{\kappa}\right)\frac{E}{RT_C{}^2}, Ln = \frac{1}{D_B},$$
$$N_A = \frac{D_T T_r}{D_B T_C \phi_r}, N_B = \frac{\Phi(\rho c)_p \phi_r}{(\rho c)_f} \tag{27}$$

The emerging normalized equations (after dropping asterisks for simplicity) are

$$\left(Pr^{-1}\frac{\partial}{\partial t} + \sigma^2 - Kr\nabla^2\right)\nabla^2 w = Ra\nabla_1^2\theta - Rn\nabla_1^2\Phi \tag{28}$$

$$\left(\frac{\partial}{\partial t} - \nabla^2\right)\theta = FKexp(\theta_b)\theta - w\frac{\partial \theta_b}{\partial z} \tag{29}$$

$$\varepsilon^{-1}w - \frac{N_A}{Ln}\nabla^2\theta - \left(\frac{1}{Ln}\nabla^2 - s\right)\Phi = 0 \tag{30}$$

Buongiorno [41] points out that Ln is of order 10^2–10^3, and N_A is <10. Employing this condition we obtain $\Phi_b = z$.

The estimate of w, θ, Φ on the boundary are

For the isothermal case (i):

$$w = 0, \quad \frac{d^2 w}{dz^2} = 0, \text{on } z = 0, 1 \tag{31a}$$

$$\frac{d\theta_b}{dz} = 0 \text{ at } z = 0, \quad \theta_b = 0 \text{ at } z = 1 \tag{31b}$$

$$\Phi = 0 \text{ on } z = 0, 1 \tag{31c}$$

For the adiabatic case (ii):

$$w = 0, \quad \frac{d^2 w}{dz^2} = 0 \text{ on } z = 0, 1 \tag{32a}$$

$$\theta = 0 \text{ on } z = 1 \text{ and } \frac{d\theta}{dz} = 0 \text{ at } z = 0 \tag{32b}$$

$$\Phi = 0 \text{ on } z = 0, 1 \tag{32c}$$

Fourier decomposition is applied to the disturbances, which reduces the perturbation equations to ordinary differential eigenvalue form. Accordingly, we assume w and θ as follows:

$$(w, \theta, \Phi) = (W(z), \Theta(z), \Sigma(z))exp[i(lx + my - \omega t)] \tag{33}$$

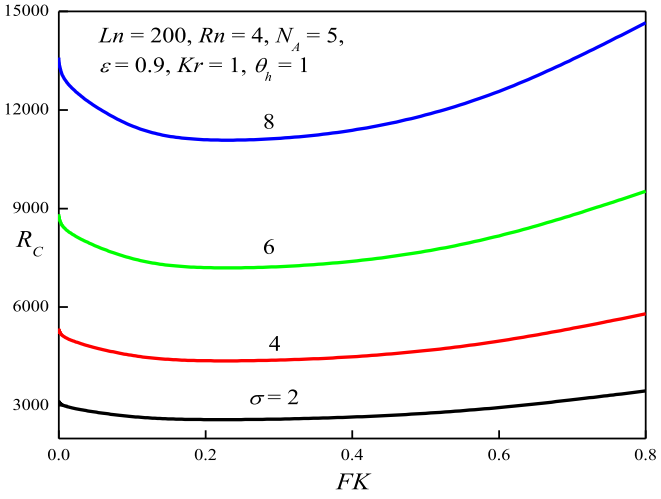

Fig. 2. R_c versus FK for various σ (isothermal case).

Here l and m are wave parameters for x and y coordinates. Using Eq. (33) in Eqs. (28)–(30) respectively, we obtain

$$\left[-iPr^{-1}\omega+\sigma^2-Kr\left(D^2-a^2\right)\right]\left(D^2-a^2\right)W=-a^2Ra\Theta+a^2Rn\Sigma \tag{34}$$

$$\left[-i\omega-\left(D^2-a^2\right)\right]\Theta=FKexp(\theta_b)\Theta-W\frac{d\theta_b}{dz}+\frac{N_B}{Ln}D\Sigma D\Theta+\frac{N_AN_B}{Ln}D\Theta D\Theta \tag{35}$$

$$\varepsilon^{-1}W-\frac{N_A}{Ln}\left(D^2-\alpha^2\right)\Theta-\left(\frac{1}{Ln}\left(D^2-\alpha^2\right)+\frac{1}{\sigma}i\omega\right)\Sigma=0 \tag{36}$$

where $a=\sqrt{l^2+m^2}$ is the horizontal wave parameter and $D\equiv\frac{d}{dz}$.

For the marginal stability where $\omega=0$, Eqs. (32)–(34) take the form

$$\left[\sigma^2-Kr\left(D^2-a^2\right)\right]\left(D^2-a^2\right)W=-a^2Ra\Theta+a^2Rn\Sigma \tag{37}$$

$$\left[\left(D^2-a^2\right)\right]\Theta-W\frac{d\theta_b}{dz}+FKexp(\theta_b)\Theta-\frac{N_B}{Ln}D\Sigma D\Theta-\frac{N_AN_B}{Ln}D\Theta D\Theta=0 \tag{38}$$

$$\varepsilon^{-1}W-\frac{N_A}{Ln}\left(D^2-\alpha^2\right)\Theta-\left(\frac{1}{Ln}\left(D^2-\alpha^2\right)\right)\Sigma=0 \tag{39}$$

Eqs. (37)–(39) with the homogeneous border conditions (31a-c) and (32a-c) define an eigenvalue problem, with modified Ra being the eigenvalue. The Galerkin method, as described in detail by Finlayson [42] is utilized to find the approximate solutions.

To, this end, we set

$$W=A_1W_1,\Theta=B_1\Theta_1 \text{ and } \Sigma=C_1\Sigma_1 \tag{40}$$

Here W_1, Θ_1 and Σ_1 are the trial functions with border conditions (31a-c) and (32a-c). Substituting Eq. (40) into Eqs. (37)–(39), multiplying the obtained equations by W_1, Θ_1 and Σ_1, respectively, integrating each equation from $z=0$ to $z=1$ we obtain:

$$A_1\left[\left(\sigma^2+2a^2Kr\right)\langle DW_1\rangle^2+a^2\left(a^2Kr+\sigma^2\right)\langle W_1{}^2\rangle+Kr\left\langle\left(D^2W_1\right)\right\rangle^2\right]-a^2RaB_1\langle W_1\Theta_1\rangle+a^2RnC_1\langle W_1\Sigma_1\rangle=0 \tag{41}$$

$$-A_1\left\langle\Theta_1W_1\frac{d\theta_b}{dz}\right\rangle-B_1\left[\left\langle(D\Theta_1)^2+a^2\Theta_1{}^2-FKexp(\theta_b)\Theta_1{}^2\right\rangle\right]=0 \tag{42}$$

$$\varepsilon^{-1}A_1\langle W_1\Sigma_1\rangle-\frac{N_A}{Ln}\left(D^2-\alpha^2\right)\langle\Theta_1\Sigma_1\rangle B_1-\left(\frac{1}{Ln}\left(D^2-\alpha^2\right)\right)\langle\Sigma_1{}^2\rangle C_1=0 \tag{43}$$

where $\langle f\rangle=\int_0^1 f\,dz$.

Eliminating A_1, B_1 and C_1 between Eqs. (41)–(43) one can find an expression for the modified Ra as (after dropping the suffixes):

$$Ra=-\frac{Ln}{a^2\langle W\Theta\rangle\left\langle W\Theta\frac{d\theta_b}{dz}\right\rangle}\left\{\begin{array}{l}\left\langle(D\Theta)^2+a^2\Theta^2-FKe^{\theta_b}\Theta^2\right\rangle\left\langle(D\Sigma)^2+(a\Theta)^2\right\rangle\\ \left[\left(\sigma^2+2a^2Kr\right)\langle DW\rangle^2+a^2\left(\sigma^2+a^2Kr\right)\langle W^2\rangle+Kr\left\langle\left(D^2W\right)^2\right\rangle\right]\\ +a^2Rn\langle W\Sigma\rangle\frac{N_A}{Ln}\left\langle W\Theta\frac{d\theta_b}{dz}\right\rangle\langle\Theta\Sigma\left(D^2-a^2\right)\rangle\\ -\varepsilon^{-1}W\Theta\left[\left\langle(D\Theta)^2+(a\Theta)^2\right\rangle\right)-\left\langle FKe^{\theta_b}\Theta^2\right\rangle\right]\end{array}\right\} \tag{44}$$

Case (i). We choose the trial functions as

$$W(z)=sin(\pi z),\Theta(z)=sin(\pi z) \text{ and } \Sigma(z)=sin(\pi z) \tag{45}$$

These satisfy the boundary conditions (31). Substituting Eq. (45) into Eq. (44) yields

$$Ra=\frac{\frac{Ln}{\varepsilon}\left(\pi^2+a^2-X\right)-\frac{\left(\pi^2+a^2\right)^2}{2}\left[\sigma^2\left(\pi^2+a^2\right)+Kr\left(\pi^2+a^2\right)^2\right]-a^2Rn\pi^4\frac{N_A}{Ln}Y\left(a^2-4\pi\right)}{a^2Y\left(\pi^2+a^2\right)} \tag{46}$$

Case (ii). We select the trial functions as

$$W(z)=sin(\pi z),\Theta(z)=sin\left(\frac{\pi}{2}z\right) \text{ and } \Sigma(z)=sin\left(\frac{\pi}{2}z\right) \tag{47}$$

These relations satisfy to the boundary conditions (32). Substituting these trial functions into the Eq. (44) yields

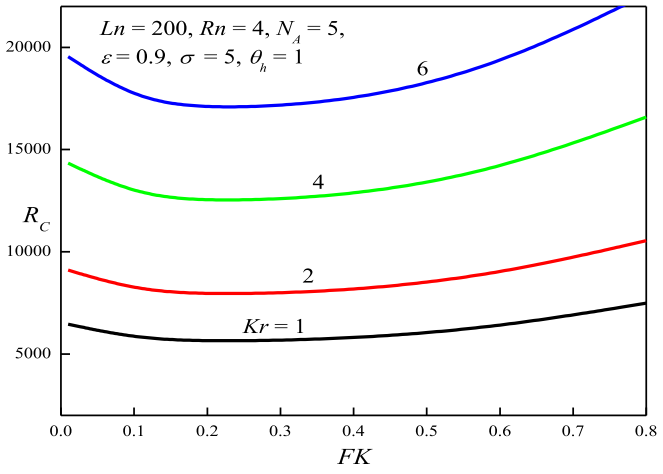

Fig. 3. R_c versus *FK* for various *Kr* (isothermal case).

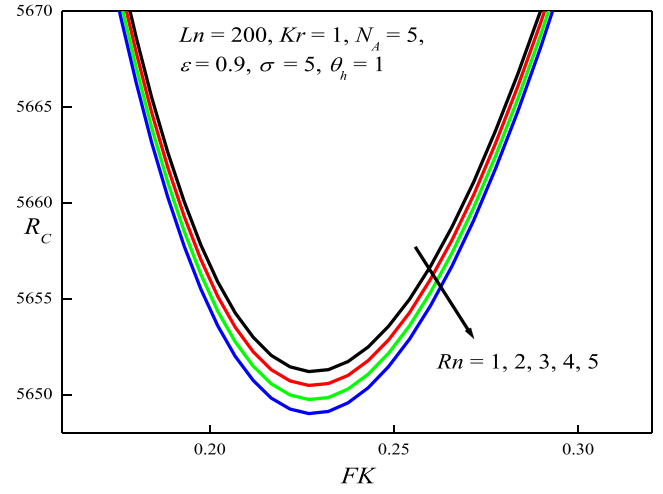

Fig. 4. R_c versus *FK* for various *Rn* (isothermal case).

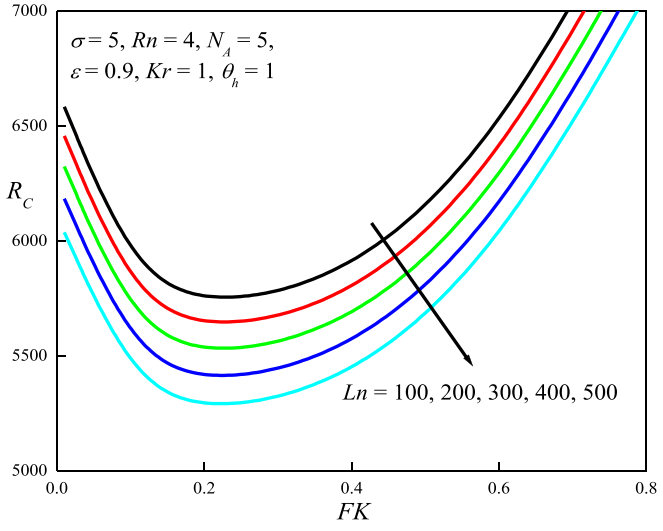

Fig. 5. R_c versus *FK* for various *Ln* (isothermal case).

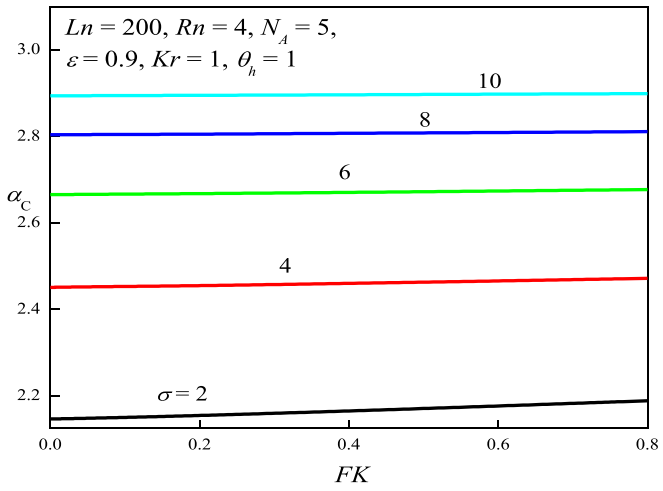

Fig. 6. α_c versus *FK* for various σ (isothermal case).

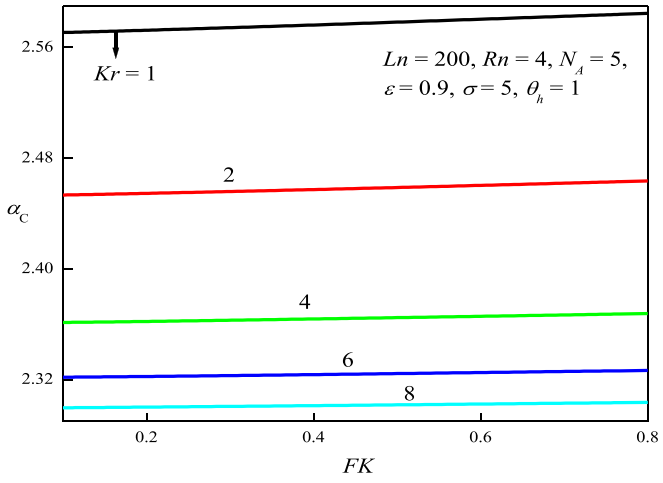

Fig. 7. α_c versus *FK* for various *Kr* (isothermal case).

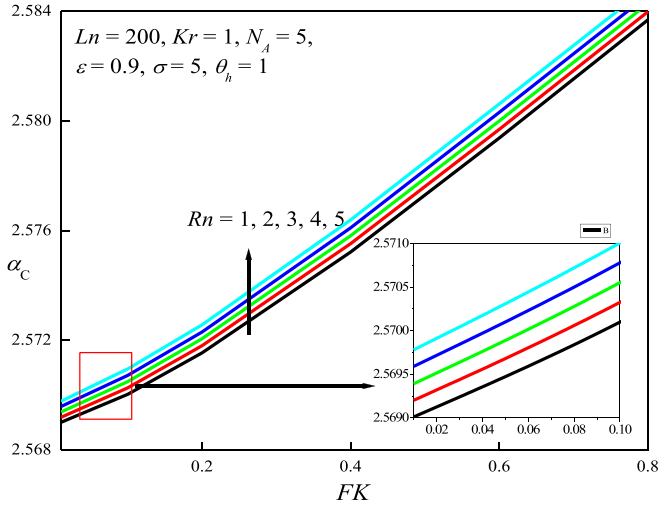

Fig. 8. α_c versus *FK* for various *Rn* (isothermal case).

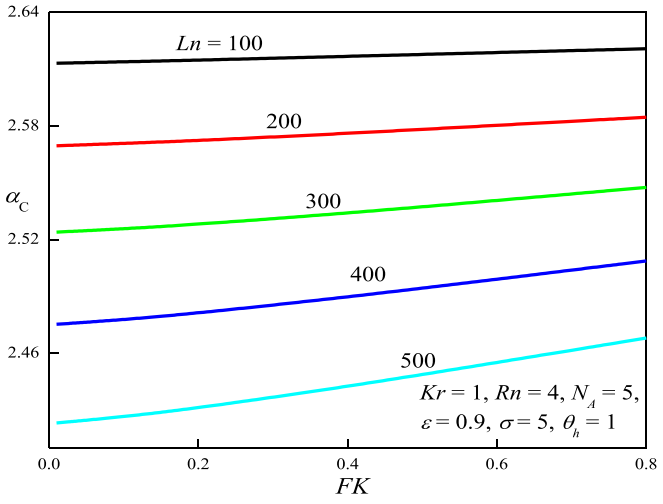

Fig. 9. α_c versus *FK* for various *Ln* (isothermal case).

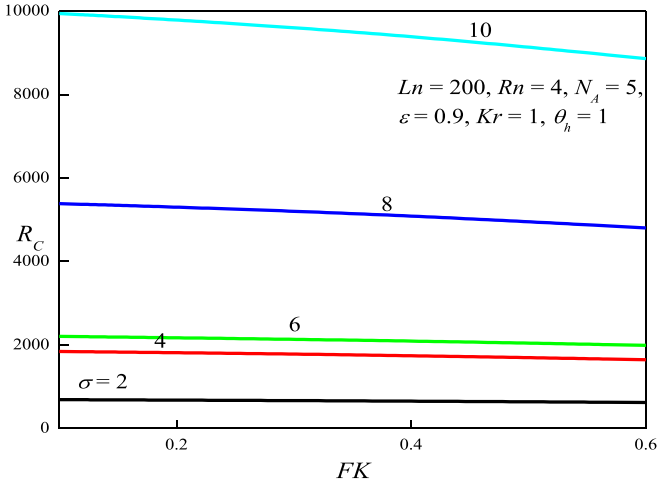

Fig. 10. R_c versus *FK* for various σ (adiabatic case).

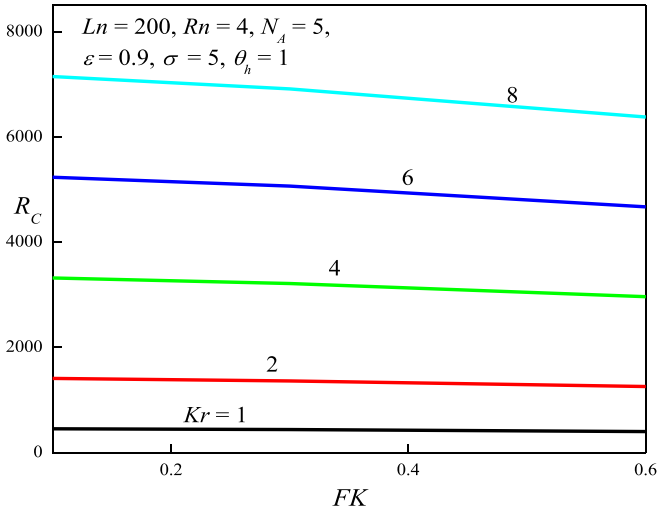

Fig. 11. R_c versus *FK* for various *Kr* (adiabatic case).

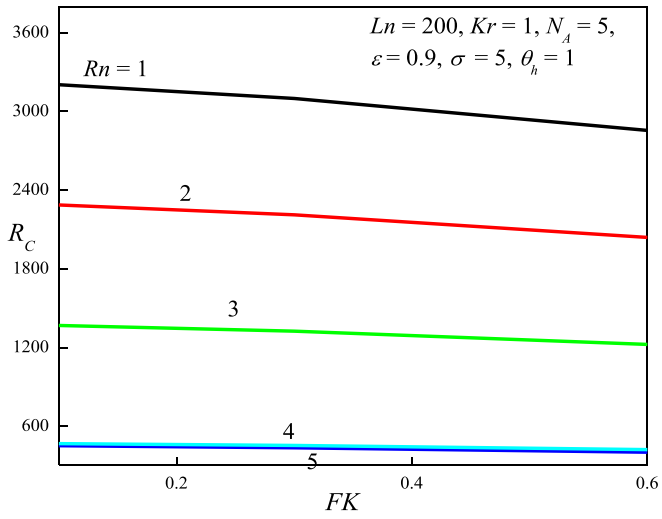

Fig. 12. R_c versus *FK* for various *Rn* (adiabatic case).

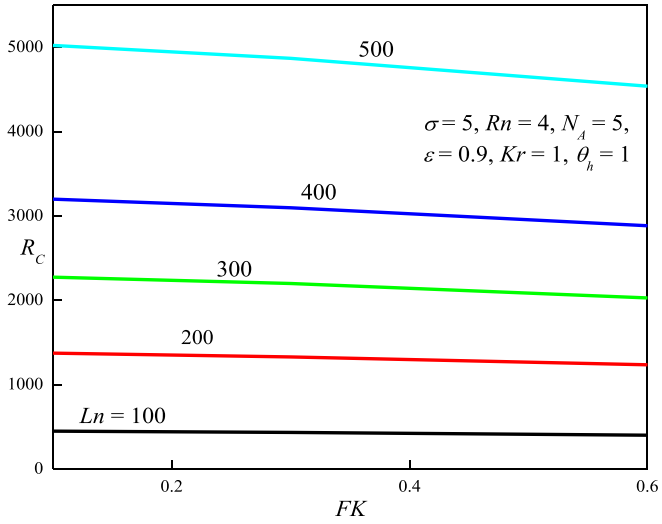

Fig. 13. R_c versus *FK* for various *Ln* (adiabatic case).

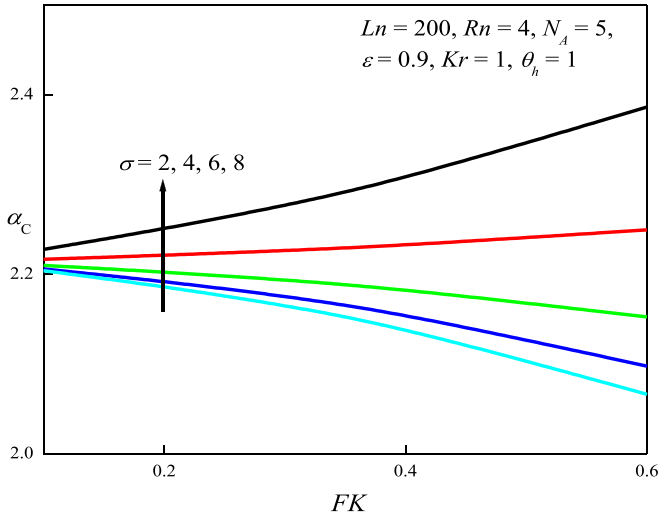

Fig. 14. α_c versus *FK* for various σ (adiabatic case).

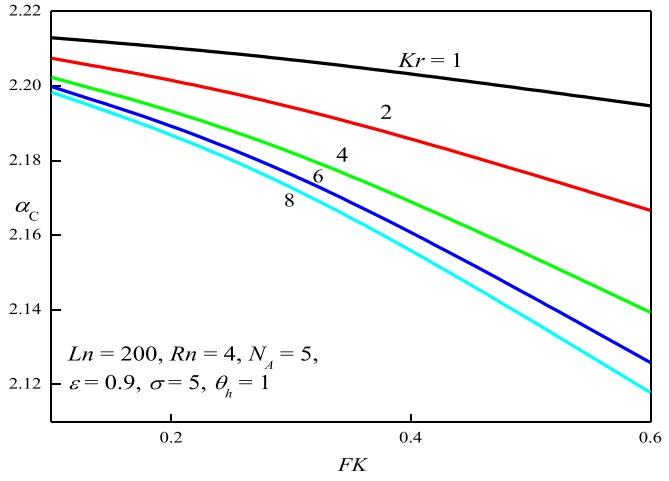

Fig. 15. α_c versus *FK* for various *Kr* (adiabatic case).

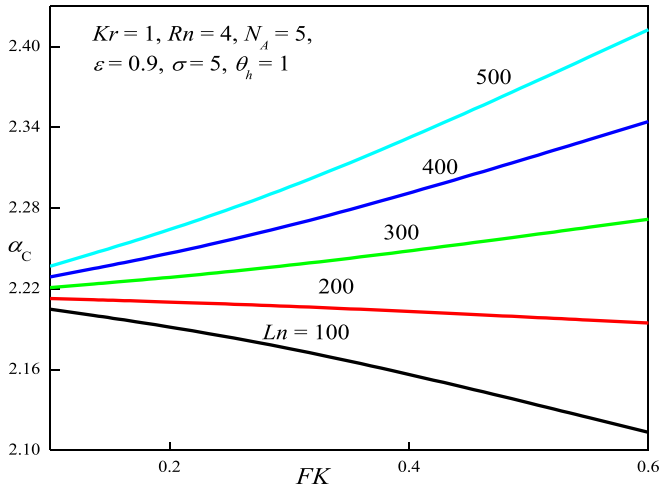

Fig. 17. α_c versus *FK* for various *Ln* (adiabatic case).

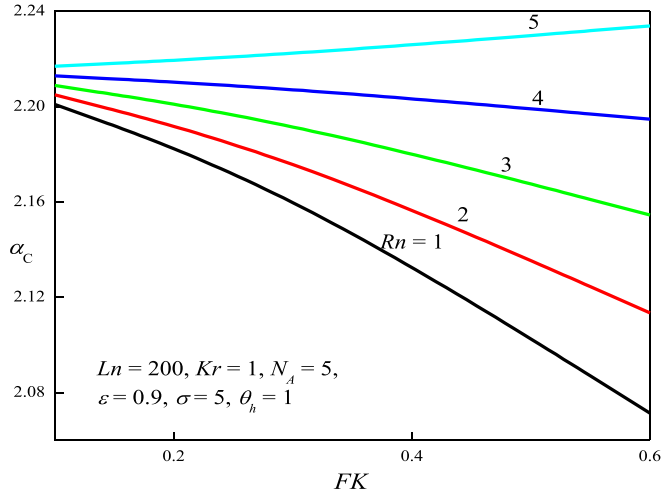

Fig. 16. α_c versus *FK* for various *Rn* (adiabatic case).

number increases, attains a minimum value and subsequently increases by rising *FK*. A critical magnitude of Frank–Kamenetskii parameter $FK = (FK)_c = 0.32$ has been determined at which the system is most unstable. This critical value $(FK)_c$ is independent of both σ and *Kr*. Furthermore, in a small range of *FK* ($0 < FK < 0.1$) Ra_c diminishes exponentially. Fig. 2 presents that increasing σ, Ra_c is boosted, prompting that porous parameter stabilizes the system (i.e. decreasing permeability), which is a classical result. We observe from Fig. 3 that developing *Kr* is to improve Ra_c indicating that large viscosity ratio is to delay convection to set on. Thus, the viscosity ratio also stabilizes the system. The outcome of *Rn* and Lewis number is shown in Figs. 4 and 5 respectively. Evidently increasing *Rn* and *Ln* reduces Ra_c suggesting that *Rn* and the Lewis number both advance the onset of convection. Thus, larger values of *Rn* and *Ln* destabilize the system.

Figs. 6–9 demonstrate the repercussion of α_c with Frank–Kamenetskii number *FK* on σ, viscosity ratio *Kr*, concentration Rayleigh number *Rn* and the Lewis number *Ln*. Figs. 6 and 7 demonstrate the enact of variation of critical wavenumber with Frank-Kamenetskii number on the porous parameter σ, viscosity ratio *Kr*, respectively. It is acquired that α_c increases with Frank–Kamenetskii number *FK* as σ is increased, hence

$$Ra = -\frac{3\pi}{4}\frac{(\pi^2+4a^2-4X)}{a^2Y(-\pi^2+a^2)}\times\begin{bmatrix} -Ln(\sigma^2+2a^2Kr)\pi^2+a^2(a^2Kr+\sigma^2)+\frac{Kr\pi^4}{4}(\pi^2+4a^2) \\ -\frac{X(\pi^2+4a^2)}{8}+\frac{4a^2RnN_AY}{3\pi Ln}-\frac{1}{\varepsilon 3\pi}(\pi^2+4a^2-4X)\end{bmatrix} \tag{48}$$

where $X = \langle 2FKe^{\theta_b}\Theta^2\rangle$, $\langle Y = W\Theta\frac{\partial\theta_b}{\partial z}\rangle$, and are computed by numerical integration. The minimum value of *Ra* for a reacting fluid is at the critical wave parameter $a = a_c$. Solving this equation for a^2 yields critical wave number a_c, which on substituting in Eq. (44), Ra_c is obtained.

4. Results and discussion

Rayleigh number has been computed for particular values of permeability parameter, viscosity ratio, nanoparticle concentration *Ra*, Lewis and Frank–Kamenetskii numbers. All the computations are visualized in Figs. 2–17 with default data.

Figs. 2–9 depict the isothermal wall conditions layouts. The change of critical *Ra* with Frank–Kamenetskii parameter for the isothermal condition for σ and *Kr* is depicted in Figs. 2 and 3 respectively. We monitor from these figures that Ra_c is reduced as Frank–Kamenetskii the porous characteristic stabilizes the onset of convection. However, the viscosity ratio *Kr* is suppressed by elaborating α_c implying that the system is destabilized. The deviation of critical wave number with *FK* on *Rn* and *Ln* is shown in Figs. 8 and 9 respectively. The impact of *Rn* is presented in Fig. 8. These figures suggest that as *Rn* is accelerated, α_c also increases i.e. greater concentration Rayleigh stabilizes the system. Fig. 9 tells that as Lewis number is gained, α_c continues to plummet, hence destabilizing or suppressing the system. The response of α_c on σ and *Kr* is similar to that computed earlier by Malashetty and Gaikwad [40]. By employing a nanoliquid, we find an enhancement in Ra_c and the wave parameter, indicating that the system is stabilized. For pure viscous fluid (i.e. when $Rn = 0$, $Ln = 0$, $N_A = 0$), the results of Malashetty and Gaikwad [40] are restored.

Figs. 10–17 depict the evolution of R_c with *FK* on σ, *Kr*, *Rn* and *Ln* for the case of an adiabatic lower boundary. It is clear that Ra_c declines as

FK raises and attains a minimum value. This behavior is similar to the isothermal wall conditions though the changes of Ra_c is not as excessive, indicating that adiabatic conditions at the base boundary lead to a less prominent modification in stability characteristics.

The Rayleigh number is assessed for separate values the porous parameter, viscosity ratio, *Rn*, *Ln* and *FK* for the adiabatic condition and the outcome are presented in Figs. 10–13. The variation of R_c with *FK* on σ and *Kr* is shown in Figs. 10 and 11. The R_c is reduced noticeably by intensifying as Frank–Kamenetskii number *FK*, decline to a minimum value and then rises by escalating the value of *FK*. This critical value $(FK)_c$ is independent of σ and *Kr*. It can also be noted that small range of *FK* ($0 < FK < 0.1$) Ra_c drops exponentially. Clearly the strength of the exothermic reaction has a marked impact on the convection and significantly alters the stability of the regime. Fig. 10 implies that the large values of σ enhances Ra_c i.e. it stabilizes the system, which as noted earlier, is a classical pattern computed in many studies of porous medium convection flows. We observe from Fig. 11 that promoting *Kr*, Ra_c is also promoted, informing that *Kr* hinder the onset of convection. Thus, greater viscosity ratio also contributes a stabilizing role on the system. The enforcement of *Rn* and *Ln* is shown in Figs. 12 and 13 respectively. From these figures, the implication is that a boost in nanoparticle concentration Rayleigh number i.e. $Rn = \left(\frac{\rho_p}{\rho_0} - 1\right)\frac{\beta g H^3 T_r}{\nu \kappa}$ is to put down Ra_c. Greater nanoparticle presence therefore is counter-productive in the adiabatic case, since it advances the onset of convection i.e. stabilizes the regime, whereas greater Lewis number constrain the onset of convection i.e. stabilizes the system.

The enact of α_c with *FK* on σ, *Kr*, *Rn* and *Ln* have been shown in Figs. 14–17. Figs. 14 and 15 model the importance of critical wave number with *FK* on σ and viscosity ratio *Kr*. The critical wave number is found to develop with Frank–Kamenetskii number as the porous parameter is enhanced; hence σ has a stabilizing effect. *Kr* is reduced for large α_c implying that higher *Kr* destabilizes the system. The response of α_c with Frank–Kamenetskii number on *Rn* and *Ln* is visualized in Figs. 16 and 17 respectively. From these, it appears that as the values of *Rn* and *Ln* are expanded, the critical wave number also increases; both concentration Rayleigh and Lewis number therefore stabilize the system.

The effects of Ra_c on σ and *Kr* concur with the computations of Malashetty and Gaikwad [40]. By using a nanofluid, we observe an enhancement in Ra_c and α_c, and hence stabilize the system. For pure viscous fluid (i.e. when the parameters $Rn = 0$, $Ln = 0$, $N_A = 0$), the results of Malashetty and Gaikwad [40] for the adiabatic case are retrieved.

5. Conclusions

The enforcement of chemical reaction on the onset of natural convection in a horizontal sparsely packed porous layer occupied by a nanoliquid, with a wall having constant temperature or thermally-insulated wall as the lower border was studied. The stability analysis was performed and the obtained eigenvalue problems were worked our approximately, using a single-term Galerkin technique with appropriate trial functions. Ra_c and its corresponding α_c are derived for distinct magnitudes of *FK*, σ, *Kr*, *Rn* and *Ln*. It was attained that the presence of multiple conductive states and the exponential dependence of the thermal production intensity on the temperature results to marked changes between reaction-driven convection and the classical Lapwood-Brinkman and Benard-type convection owing to an applied temperature drop. The chemical reaction results in a distributed energy source which causes for the nonlinear temperature distribution in the base state. Hence chemical reaction advances the onset of convection when correlated with no chemical reaction. The following conclusions are drawn:

(i) The exothermic chemical reaction is to accelerate the onset of convection for a certain range of *FK*. The critical magnitude of *FK* exists $FK = (FK)_c$ where the system is most unstable which is independent on *Kr* and σ.
(ii) Increasing the viscosity ratio is to postpone the onset of convection.
(iii) The influence of Ra_c on the porous medium parameter σ and the viscosity ratio *Kr* is the similar observations mady by Malashetty and Gaikwad [40] for both isothermal and adiabatic cases.
(iv) The critical wave number on the porous medium parameter σ and the viscosity ratio *Kr* is the same as defined by Malashetty and Gaikwad [40] for both isothermal and adiabatic cases.
(v) For pure viscous fluid (i.e. $Rn = 0$, $Ln = 0$, $N_A = 0$), we obtain the same results of Malashetty and Gaikwad [40] for isothermal and the adiabatic case.
(vi) By using a nanofluid i.e. doping viscous fluid with nanoparticles, an enhancement is achieved on Ra_c and α_c, thereby augmenting the stability of the regime.

The present investigation has acknowledged the interesting thermosolutal fluid dynamic stability characteristics of relevance to geothermal energy systems and chemical reactors. However, simulations have been confined to Newtonian flows. Future investigations may consider non-Newtonian models (Giraldo et al., [43]) for nanofluid thermal ignition reaction flows, which are also useful in geothermal systems and reactor designs.

CRediT authorship contribution statement

J.C. Umavathi: Conceptualization, Methodology, Data curation, Writing – original draft, Writing – review & editing. **M.A. Sheremet:** Writing – original draft, Writing – review & editing.

Declaration of Competing Interest

None.

Acknowledgements

This research of M.A. Sheremet was supported by the Tomsk State University Development Programme (Priority-2030).

References

[1] D. Sui, V.H. Langakar, Z. Yu, Investigation of thermophysical properties of nanofluids for application in geothermal energy, Energy Procedia 105 (2017) 5055–5060.
[2] M. Daneshipour, R. Rafee, Nanofluids as the circuit fluids of the geothermal borehole heat exchangers, Int. Commun. Heat Mass Transf. 81 (2017) 34–41.
[3] M. Faizal, B. Abdelmalek, M.S. Rao, Heat transfer enhancement of geothermal energy piles, Sustain. Energy Rev. 57 (2016) 16–33.
[4] K. Bucher, I. Stober, Large scale chemical stratification of fluids in the crust: hydraulic and chemical data from the geothermal research site Urach Germany, Geofluids 16 (2016) 813–825.
[5] R. Rana, R.N. Home, P. Cheng, Natural convection in a multi layered geothermal reservoir, ASME, J. Heat Transf. 101 (1979) 411–416.
[6] G. Schubert, J.M. Straus, Gravitational stability of water over steam in vapor-dominated Geothermal systems, J. Geophys. Res. 85 (1980) 6505–6512.
[7] Q. Gan, Q. Lei, Induced fault reactivation by thermal perturbation in enhanced geothermal systems, Geothermics 86 (2020), 101814.
[8] R.O. Fournier, Double-diffusive convection in geothermal systems: the salton sea, California, geothermal system as a likely candidate, Geothermics 19 (1990) 481–496.
[9] D.A. Frank-Kamenetskii, Diffusion and Heat Transfer in Chemical Kinetics, 2nd edition, Plenum Press, USA, 1969.
[10] C.K. Law, H.K. Law, Thermal-ignition analysis in boundary-layer flows, J. Fluid Mech. 92 (1979) 97–108.
[11] S. Li, Q. Yao, C.K. Law, Thermal-ignition analysis in wall-bounded boundary-layer flows with an unheated starting length, Combust. Sci. Technol. 190 (2018) 1722–1737.
[12] O.A. Bég, M.M. Rashidi, M. Keimanesh, T.A. Bég, Semi-numerical modelling of "chemically frozen" combusting buoyancy-driven boundary layer flow along an inclined surface, Int. J. Appl. Math. Mech. 9 (2013) 1–16.

[13] O.A. Bég, S.S. Motsa, M.N. Islam, M. Lockwood, Pseudo-spectral and variational iteration simulation of exothermically reacting Rivlin-Ericksen viscoelastic flow and heat transfer in a rocket propulsion, Comput. Thermal Sci. 6 (2014) 91–102.
[14] M.S. Hashmi, N. Khan, S.U. Khan, M.M. Rashidi, A mathematical model for mixed convective flow of chemically reactive Oldroyd-B fluid between isothermal stretching disks, Results Phys. 7 (2017) 3016–3023.
[15] P. Gordon, On thermal explosion in porous media, Nonlinearity 23 (2010) 1433–1449.
[16] M.M. Rahman, I. Pop, M.Z. Saghir, Steady free convection flow within a titled nanofluid saturated porous cavity in the presence of a sloping magnetic field energized by an exothermic chemical reaction administered by Arrhenius kinetics, Int. J. Heat Mass Transf. 129 (2019) 198–211.
[17] R. Ul-Haq Muhammad, Analysis of heat transfer in a triangular enclosure filled with a porous medium saturated with magnetized nanofluid charged by an exothermic chemical reaction, Math. Probl. Eng. 2019 (2019), 7451967.
[18] W. Kordylewski, Z. Krajewski, Convection effects on thermal ignition in porous media, Chem. Eng. Sci. 39 (1984) 610–612.
[19] J.E. Gatica, H.J. Viljoen, V. Hlavacek, Stability analysis of chemical reaction and free convection in porous media, Int. Comm. Heat Mass Transfer 14 (1987) 391–403.
[20] K. Vafai, C.P. Desai, S.C. Chen, An investigation of heat transfer process in a chemically reacting packed bed, Num. Heat Transfer 124 (1993) 127–142.
[21] S. Subramanian, V. Balakotaiah, Convective instabilities induced by exothermic reactions occurring in a porous medium, Phys. Fluids 6 (1994) 2907–2922.
[22] M.S. Malashetty, P. Cheng, B.H. Chao, Convective instability in a horizontal porous layer saturated with a chemically reacting fluid, Int. J. Heat Mass Transf. 37 (1994) 2901–2908.
[23] N. Kladias, V. Prasad, Flow transitions in a buoyancy-induced non-Darcy convection in a porous medium heated from below, ASME, J. Heat Transf. 112 (1990) 675–684.
[24] P. Vasseur, L. Robillard, The Brinkman model for natural convection in a porous layer: Effects of non-uniform thermal gradient, Int. J. Heat Mass Transf. 36 (1993) 4199–4206.
[25] O.A. Bég, Takhar Prasad, V.M. Soundalgekar, Thermo-convective flow in an isotropic, homogenous medium using Brinkman's model: numerical study, Int. J. Num. Methods Heat Fluid Flow 8 (1998) 59–89.
[26] J.P. Kumar, J.C. Umavathi, Y. Ramarao, Free and forced convective flow in a vertical channel filled with composite porous medium using Robin boundary conditions, Am. J. Appl. Mathe. 2 (2014) 96–110.
[27] D. Tripathi, O.A. Bég, A numerical study of oscillating peristaltic flow of generalized Maxwell viscoelastic fluids through a porous medium, Transp. Porous Media 95 (2012) 337–348.
[28] N. Alsedais, A.M. Aly, M.A. Mansour, Local thermal non-equilibrium condition on mixed convection of a nanofluid-filled undulating cavity containing obstacle and saturated by porous media, Ain Shams Eng. J. 13 (2) (2022), 101562.
[29] A.M. Aly, S. El-Sapa, Effects of Soret and Dufour numbers on MHD thermosolutal convection of a nanofluid in a finned cavity including rotating circular cylinder and cross shapes, Int. Comm. Heat Mass Transfer 130 (2022), 105819.
[30] A.M. Aly, A.M. Yousef, N. Alsedais, MHD double diffusion of a nanofluid within a porous annulus using a time fractional derivative of the ISPH method, Int. J. Modern Phys. C 33 (4) (2022), 2250056.
[31] N. Alsedais, A.M. Aly, Double-diffusive convection from an oscillating baffle embedded in an astroid-shaped cavity suspended by nano encapsulated phage change materials: ISPH simulations, Waves Random Complex Media (2021), https://doi.org/10.1080/17455030.2021.1994168.
[32] N. Singh, M.K. Khandelwal, Linear stability perspective on mixed convection flow of nanofluids in a differentially heated vertical channel, Int. Comm. Heat Mass Transfer 134 (2022), 105989.
[33] X. Zhou, F. Chi, Y. Jiang, Q. Chen, Numerical investigation of thermocapillary convection instability for large Prandtl number nanofluid in rectangular cavity, Int. Comm. Heat Mass Transfer 133 (2022), 105956.
[34] Y.P. Hu, F.J. Wang, Y.C. Zhang, Y.R. Li, M.H. Li, Oscillatory natural convection of Al_2O_3-water nanofluid near its density maximum in a narrow horizontal annulus, Int. Comm. Heat Mass Transfer 136 (2022), 106207.
[35] B.S. Bhadauria, P. Kiran, Heat and mass transfer for oscillatory convection in a binary visco-elastic fluid layer subject to temperature modulations at the boundaries, Int. Comm. Heat Mass Transfer 58 (2014) 166–175.
[36] J. Liu, P.A. Garcia-Salaberri, I.V. Zenyuk, The impact of reaction on the effective properties of multiscale catalytic porous media: a case of polymer electrolyte fuel cells, Transp. Porous Media 128 (2019) 363–384.
[37] O.M. Phillips, Geological Fluid Dynamics-Sub-Surface Flow and Reactions, Cambridge University Press, 2009.
[38] F. Stroh, V. Balakotaiah, Stability of uniform flow in packed-bed reactors, Chem. Eng. Sci. 47 (1992) 593–604.
[39] S. Subramanian, V. Balakotaiah, Convective instabilities induced by exothermic reactions occurring in a porous medium, Phys. Fluids 6 (1994) 2907–2922.
[40] M.S. Malashetty, S.N. Gaikwad, Onset of convection in a horizontal porous layer saturated with reacting fluid, Int. J. Trans. Phenomena 1 (2007) 1–9.
[41] J. Buongiorno, Convective transport in nanofluids, ASME J. Heat Transf. 128 (2006) 240–250.
[42] B.A. Finlayson, The Galerkin method applied to convective instability problems, J. Fluid Mech. 33 (1968) 201–208.
[43] L.J. Giraldo, M.A. Giraldo, S. Llanos, G. Maya, R.D. Zabala, N.N. Nassar, C. A. Franco, V. Alvarado, F.B. Cortes, The effects of SiO_2 nanoparticles on the thermal stability and rheological behaviour of hydrolyzed polyacrylamide based polymeric solutions, J. Pet. Sci. Eng. 159 (2017) 841–852.